

Original paper

Crystal structure of synthetic “magnesorietveldite”, Raman spectroscopy data and bond-valence approach to the svornostite group of minerals

Jakub PLÁŠIL^{1*}, Radek ŠKODA², Anthony R KAMPF³, Ivan NĚMEC⁴, Nicolas MEISSER⁵ and Georges FAVREAU⁶

¹ Institute of Physics of the CAS, Na Slovance 2, 182 00 Prague 8, Czech Republic, plasil@fzu.cz

² Department of Geological Sciences, Masaryk University, Kotlářská 2, CZ-61137 Brno, Czech Republic

³ Mineral Sciences Department, Natural History Museum of Los Angeles County, 900 Exposition Boulevard, Los Angeles, CA 90007, USA

⁴ Department of Inorganic Chemistry, Faculty of Science, Charles University, Hlavova 8, 128 00 Prague 2, Czech Republic

⁵ Département de géologie, Muséum cantonal des sciences naturelles (Naturéum), Université de Lausanne (UNIL), Anthropole, 1015 Lausanne, Switzerland

⁶ independent researcher, 421, avenue Jean Monnet, 13090 Aix-en-Provence, France

* Corresponding author



The new synthetic counterpart of a potentially new member of the svornostite group of minerals, “magnesorietveldite”, ideally $\text{Mg}(\text{UO}_2)(\text{SO}_4)_2(\text{H}_2\text{O})_3$, is orthorhombic, space group $Pmn2_1$, $a = 12.7950(9)$, $b = 8.3288(4)$, $c = 11.2962(4)$ Å, $V = 1203.80(11)$ Å³ and $Z = 2$. The crystal structure ($R_1 = 0.0168$ for 3113 $I > 3\sigma I$ reflections) contains uranyl-sulfate chains that are linked into sheets by $\text{M1O}_2(\text{H}_2\text{O})_4$ and $\text{M2O}_2(\text{H}_2\text{O})_4$ octahedra, where Mg is a dominant cation over Zn at both sites. The structure is well known and has already been described for other members of the svornostite group; the fundamental building unit – an infinite $[(\text{UO}_2)(\text{SO}_4)_2(\text{H}_2\text{O})]^{2-}$ chain – is common in several uranyl minerals and synthetic compounds. Synthetic “magnesorietveldite” was obtained after treatment of a specimen containing pitchblende with sulfuric acid. Electron microprobe analyses yielded the empirical formula $(\text{Mg}_{0.63}\text{Zn}_{0.22}\text{Cu}_{0.09}\text{Fe}_{0.05})_{\Sigma 0.99}(\text{UO}_2)(\text{SO}_4)_2 \cdot 5\text{H}_2\text{O}$, confirming the predominance of Mg over the other divalent cations. Infrared and Raman spectroscopy confirmed the presence of structurally non-equivalent molecular H_2O and sulfate tetrahedra. We append an extensive discussion on the role of molecular H_2O in the svornostite-group of minerals based on the bond-valence approach.

Keywords: magnesorietveldite, svornostite group, uranyl sulfate, crystal structure, Raman spectroscopy

Received: 12 November 2025; **accepted:** 18 December 2025; **handling editor:** J. Sejkora

We dedicate this paper to the memory of Ing. Jiří Čejka, DrSc. (1929–2025), our dear colleague, mentor, and friend, who was convinced of the importance of weakly bonded constituents in uranyl oxysalts more than 60 years ago.

1. Introduction

Natural and synthetic uranyl sulfates are of interest because they lie at the confluence between uranium chemistry, geochemistry/mineralogy, and industrial/environmental issues. Over the past twenty years, research on these phases has yielded important insights into mineralogical geodiversity and crystallography (Plášil 2014; Gurzhiy and Plášil 2019; Plášil et al. 2023).

Synthetic uranyl sulfates are used as precursors for treating uranium ore or uranium-bearing metallurgical waste. The leaching agent is sulphuric acid, which dissolves uranium under oxidizing conditions, forming soluble, highly stable uranyl sulfates. This step is essential before uranium can be extracted by ion exchange or precipitation.

Both in uranium deposits that have never been mined and in abandoned mining sites, uranyl sulfates are com-

mon and form in acid drainage: the oxidation of sulfides (pyrite, chalcopyrite, etc.) produces sulfuric acid, which mobilizes uranium. The uranyl sulfates are highly soluble and mobile, making them one of the most concerning forms of uranium pollution in acidic waters. Through capillary action and evaporation, these solutions deposit crystals of hydrated uranyl sulfates and, in general, other oxysalts. Studying them is therefore essential for predicting uranium dispersion in the biosphere and for developing remediation methods (e.g., Brugger et al. 2003; Plášil et al. 2014, 2022; Majzlan et al. 2014).

Over the last decade, the search for new natural uranyl minerals in inactive uranium mines, particularly in the Czech Republic (Jáchymov) and the USA (Red Canyon, southeastern Utah), yielded an immense number of new uranyl sulfate minerals (Fig. 1) (e.g., Plášil et al. 2023 and references therein). In abandoned mines, optimal

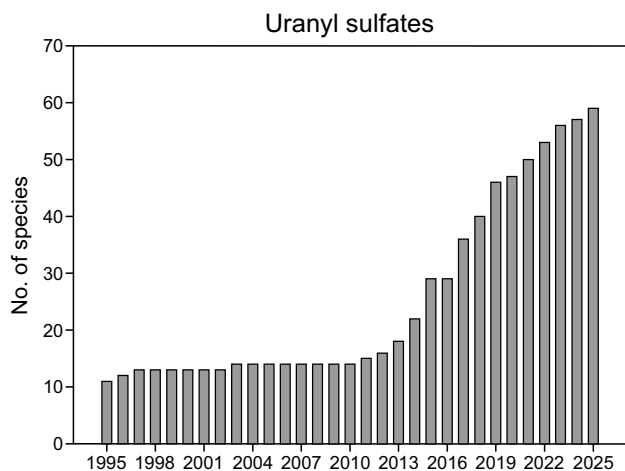


Fig. 1 The number of known uranyl sulfate minerals over the 1995–2025 timespan, with an astonishing increase over the past decade, primarily due to discoveries in Jáchymov (CZ) and localities in Utah and Colorado (USA).

conditions for the growth of secondary minerals exist due to high relative air humidity and stable temperatures. Crystallographic studies on these new minerals have revealed some exciting features not previously observed in either natural or synthetic phases (Gurzhiy and Plášil 2019).

In 2015, the new mineral svornostite, $K_2Mg(UO_2)_2(SO_4)_4(H_2O)_8$, was described by Plášil et al. (2015) from Jáchymov, Czech Republic. Its structure is based on infinite $[(UO_2)(SO_4)_2(H_2O)]^{2-}$ chains interlinked by $MgO_2(H_2O)_4$ octahedra. The structure is very similar to that of a group of synthetic compounds with the general formula, originally given as $M^{2+}(UO_2)(SO_4)_2 \cdot 5H_2O$, and

described by Serezhkin and Serezhkina (1978). In 2017, Kampf et al. (2017) described a mineral named rietveldite, $Fe^{2+}(UO_2)(SO_4)_2(H_2O)_5$. It originates from three localities: the Giveaway-Simplot mine in Utah (USA), the Willi Agatz mine in Saxony (Germany), and Jáchymov (Western Bohemia, Czech Republic). The structures of rietveldite and svornostite are almost identical, except that one of the octahedrally coordinated Fe sites and two H_2O sites present in the rietveldite structure are missing in the svornostite structure, being replaced by K sites. Kampf et al. (2017) also noted that the structures of rietveldite and the synthetic $M^{2+}(UO_2)(SO_4)_2 \cdot 5H_2O$ of Serezhkin and Serezhkina (1978) compounds are, in fact, polytypes. Rietveldite has approximately doubled the a cell parameter of the synthetic compounds. Plášil et al. (2023) described oldsite, $K_2Fe^{2+}(UO_2)_2(SO_4)_4(H_2O)_8$, from the North Mesa mine group (Utah, USA), a Fe^{2+} -analogue of svornostite. That same year, Kampf et al. (2023) described the Zn-analogue of rietveldite, zincrietveldite, $Zn(UO_2)(SO_4)_2(H_2O)_5$, from the Blue Lizard mine (Utah, USA). Finally, in 2025, Kampf et al. (2025) described the NH_4^+ -analogue of svornostite, $(NH_4)_2Mg(UO_2)_2(SO_4)_4(H_2O)_8$, which is named svornostite- (NH_4) in line with a new group nomenclature scheme for these closely related minerals (for details, see Kampf et al. 2025). Natural “magnesorietveldite” is more than expected species (given the existing rietveldite with octahedrally coordinated Fe or Zn), but it has not been unambiguously confirmed in nature. Here, we present crystallographic, chemical, and vibrational spectroscopy data for the “magnesorietveldite” synthetic counterpart.



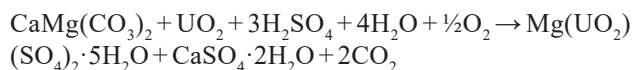
2. Samples

The specimen treated to produce synthetic “magnesorietveldite” originates from Lodève, France. It is a $3 \times 2.5 \times 1.5$ cm piece of dolomitic matrix containing fine-grained uraninite. The specimen was treated with mild H_2SO_4 acid during a leaching experiment conducted by one of the authors (GF). After treatment, the surface of the specimen was covered with gypsum crystals (colorless) and pale-yellow,

Fig. 2 Tabular crystals of synthetic “magnesorietveldite” with apparent orthorhombic shapes. Specimen MGL 086998 (anthropotype); horizontal field of view is 5 mm (photo by Stefan Ansermet).

translucent-to-transparent “magnesorietveldite” crystals (reaching up to 0.5–1 mm across) (Fig. 2).

The reaction responsible for the formation of the “magnesorietveldite” and gypsum is:



The specimen is deposited in the Muséum cantonal des sciences naturelles (Naturéum), Université de Lausanne (UNIL), under the registration number MGL 086998 (anthropotype).

3. Infrared and Raman spectroscopy of synthetic “magnesorietveldite”

Infrared spectra of synthetic “magnesorietveldite” (Figs 3, 4) were recorded on a Thermo Fisher Scientific Nicolet iN10 FTIR microscope by ATR technique (Ge crystal) in the 4000–675 cm^{-1} region (4 cm^{-1}

resolution, 128 scans, Norton–Beer strong apodization) using an MCT detector. Standard ATR correction (Thermo Nicolet Omnic 9.2 software) was applied to the recorded spectra.

Raman spectra (Figs 5, 6) were obtained from a loose crystal by means of a Horiba Labram HR Evolution spectrometer. This dispersive, edge-filter-based system is equipped with an Olympus BX 41 optical microscope, a diffraction grating with 600 grooves per millimetre, and a Peltier-cooled, Si-based charge-coupled device (CCD) detector. The Raman signal was excited by a 532 nm laser. The nominal laser beam energy of 50 mW was attenuated to 10% using a neutral density filter to avoid the thermal damage of the analysed area. The Raman spectrum was collected in the range 4000–50 cm^{-1} with a 50× objective and the system operated in confocal mode. The beam diameter was $\sim 2.6 \mu\text{m}$, and the axial resolution $\sim 5 \mu\text{m}$. Time acquisition was 60 s per spectral window, 5 accumulations, and 7 spectral windows were applied to cover the 4000–50 cm^{-1} range. Wavenumber calibration was done using the Rayleigh line and low-pressure Ne-lamp emis-

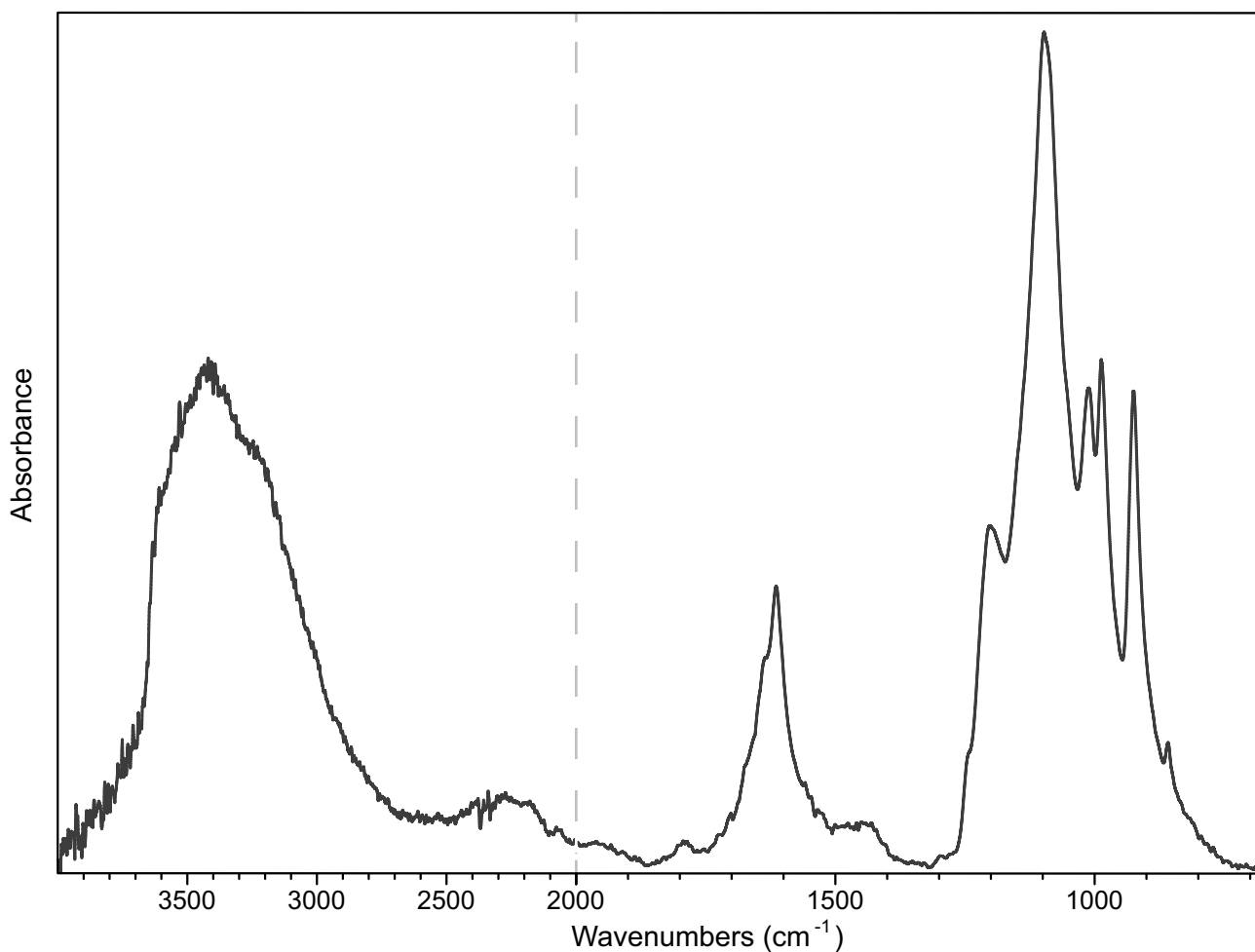


Fig. 3 Infrared spectrum of a synthetic “magnesorietveldite” collected in ATR mode (split at 2000 cm^{-1}).

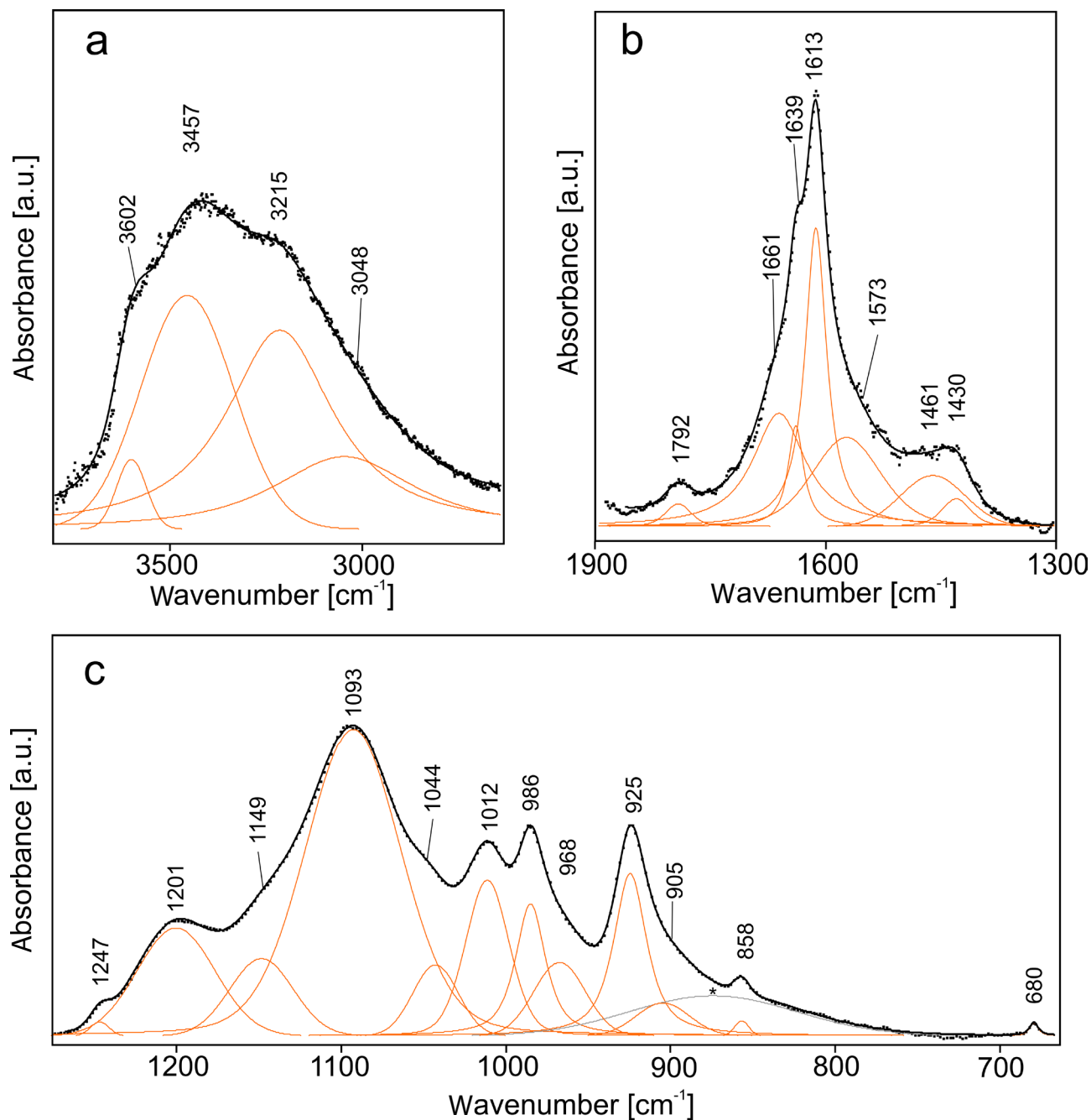


Fig. 4 Infrared spectral fitting of synthetic “magnesorietveldite”. **a** – O–H stretching region. **b** – H₂O bending region. **c** – 1300–675 cm⁻¹ region. The experimental spectrum is shown by dots. The curve matching the dots is a result of a spectral fit as a sum of individual Voigt peaks shown below the curve. The very broad hump marked by an asterisk likely does not represent a vibrational band, but may result from an instrument-related artifact or improper background subtraction.

sions. The wavenumber accuracy was ~ 0.5 cm⁻¹, and the spectral resolution was ~ 2 cm⁻¹. Raman spectra were collected in two polarization geometries: (i) with the electric vector of the incident laser beam parallel to the elongation of the crystal ($E \parallel c$ geometry), and (ii) with E oriented perpendicular to the elongation ($E \perp c$ geometry).

Band fitting of infrared and Raman spectra (Figs 4, 6) was done after background subtraction, assuming com-

bined Lorentzian-Gaussian band shapes using the Voigt function (*PeakFit*; Jandel Scientific Software).

The infrared and Raman spectra of synthetic “magnesorietveldite” are very similar to those previously reported for rietveldite and zincorietveldite (Kampf et al. 2017, 2023) and show features comparable to other hydrated uranyl sulfates (e.g., Čejka 1999, Čejka et al. 2009, Vlček et al. 2009). The infrared and Raman bands

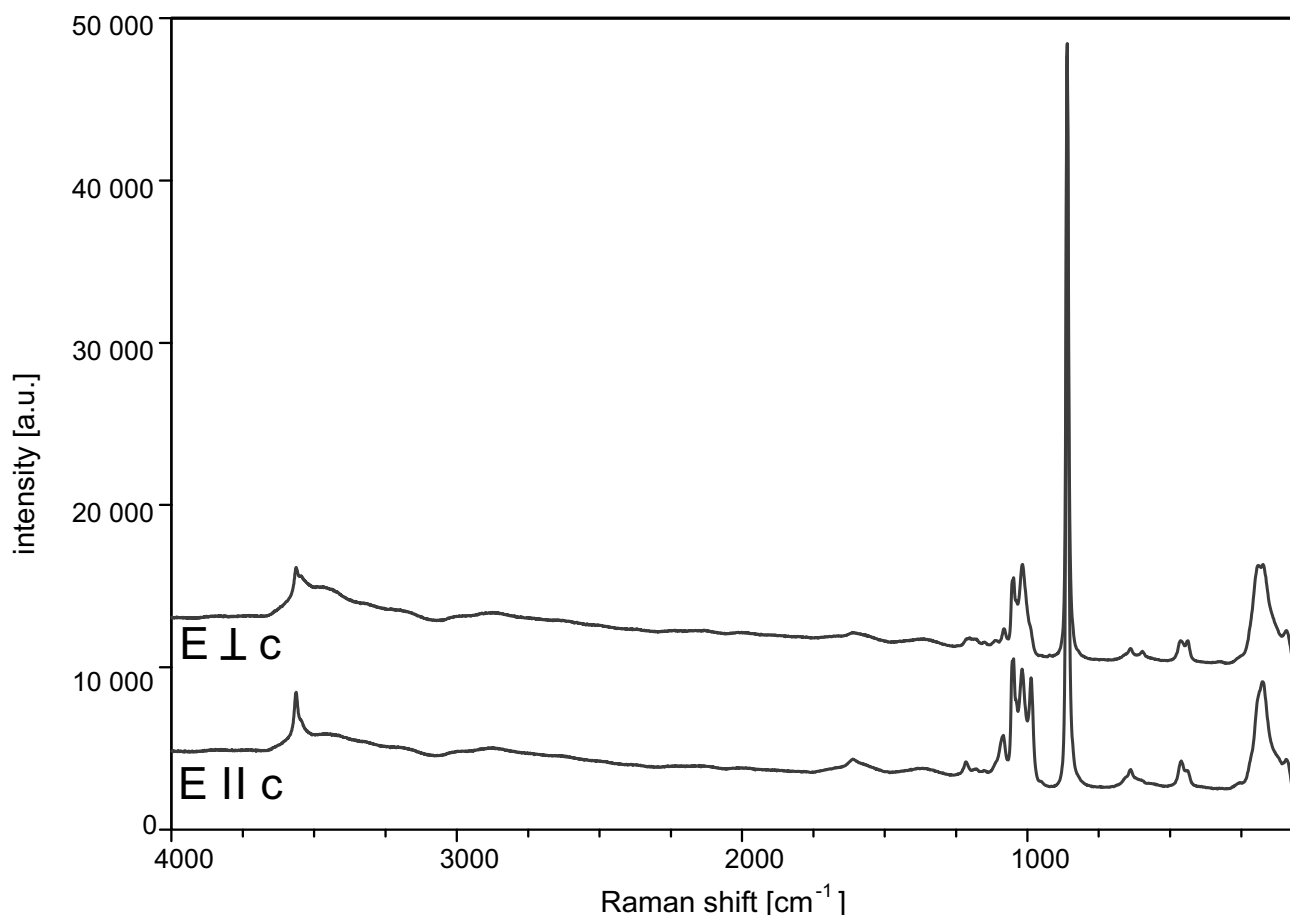


Fig. 5 Raman spectra of the synthetic “magnesorietveldite” excited with a 532 nm laser, collected in E ∥ c and E ⊥ c polarization geometries.

of synthetic “magnesorietveldite” were interpreted using the aforementioned studies.

3.1. O–H vibrations

The bands at 3602, 3457, 3215, and 3048 cm^{-1} in the infrared spectra and corresponding Raman bands at 3604, 3564, 3549, 3462, 3307, and 3195 cm^{-1} are assigned to ν (O–H) stretching vibrations of hydrogen-bonded H_2O in structurally non-equivalent sites. Raman band at 3462 cm^{-1} is significantly weaker in the E ∥ c polarization geometry. Following the empirical relationship determined by Libowitzky (1999), the O–H \cdots O hydrogen bond lengths were inferred from the respective wavenumbers (except for bands ≥ 3592 cm^{-1}) to be approximately 2.84, 2.71, and 2.66 Å for infrared bands and 3.05, 3.00, 2.85, 2.75, and 2.70 Å for Raman bands. These values are comparable with those obtained from the single-crystal X-ray diffraction for those O \cdots O involved in hydrogen bonding.

The infrared bands at 1661, 1639, 1613, and 1573 cm^{-1} (Fig. 4b) and the corresponding weaker Raman bands at 1669, 1612, and 1568 cm^{-1} (Fig. 6b) are assigned to the ν_2 bending vibrations of H_2O molecules.

The latter are more pronounced in the E ∥ c polarization geometry.

3.2. SO_4^{2-} vibrations

The overlapping infrared bands at 1247, 1201, 1149, 1093, and 1044 cm^{-1} are attributed to the triply degenerate ν_3 antisymmetric stretching vibrations of two $(\text{SO}_4)^{2-}$ units, whereas the bands at 1012, 986, 968 cm^{-1} are assigned to ν_1 symmetric stretching modes. The lowering of the ideal T_d symmetry of the $(\text{SO}_4)^{2-}$ ions induces the splitting of degenerate modes, making them active in infrared and Raman spectra, and accounts for the high number of observed sulphate bands. In the Raman spectra, the ν_3 stretching vibrations are represented by weak to medium-intense bands at 1215, 1182, 1151, 1105, 1086, 1055, 1048, and 1039 cm^{-1} , whereas the bands at 1019, 1002, and 986 cm^{-1} are linked to ν_1 vibrations.

Raman bands at 661, 639, and 594 cm^{-1} are attributed to the triply degenerate ν_4 antisymmetric bending vibrations of $(\text{SO}_4)^{2-}$, while the bands at 462 and 439 cm^{-1} correspond to the doubly degenerate ν_2 bending vibrations.

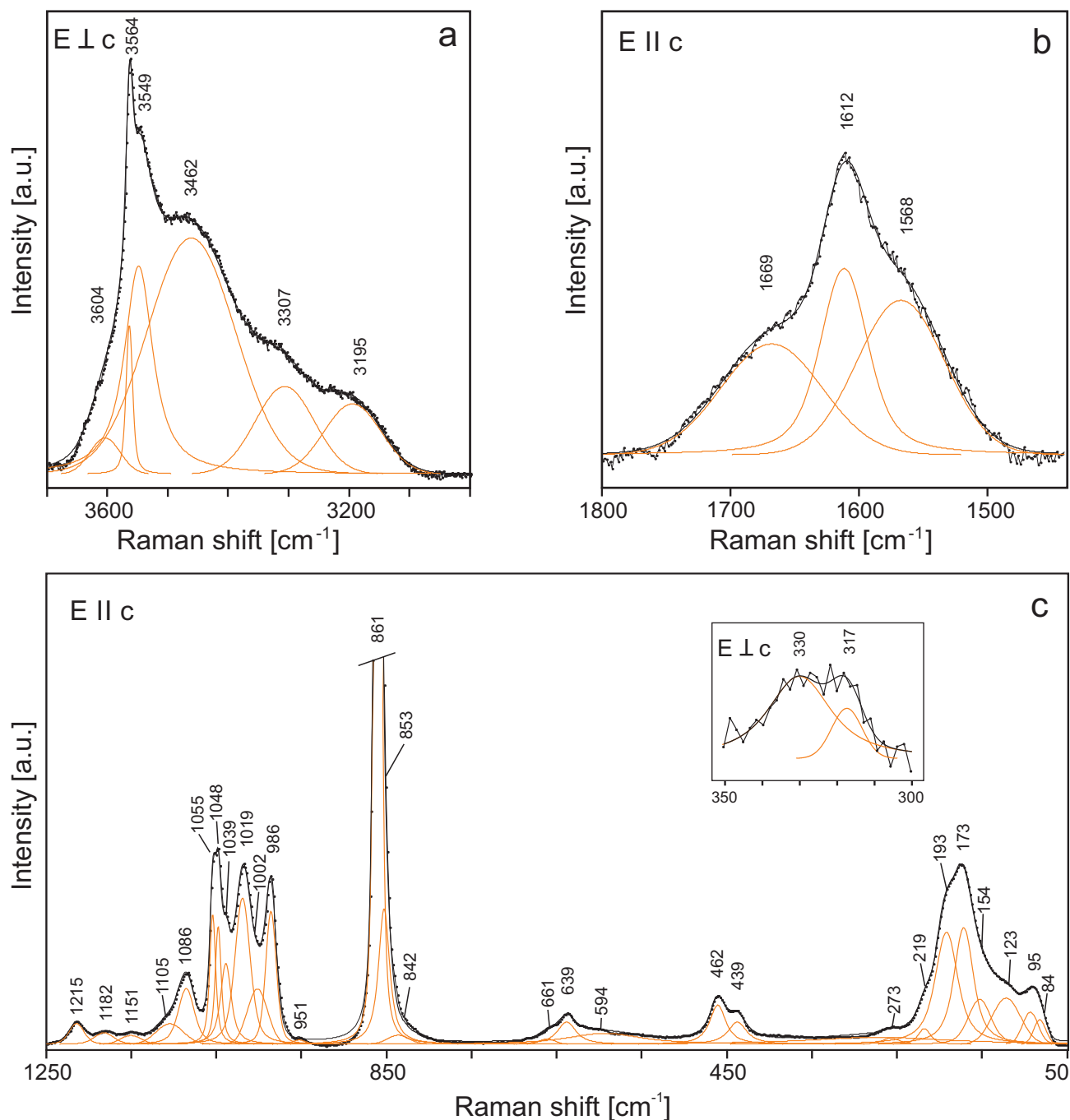


Fig. 6 Raman spectral fitting of synthetic “magnesorietveldite”. **a** – O–H stretching region collected in the $E \perp c$ polarization geometry. **b** – H_2O bending region collected in the $E \parallel c$ polarization geometry. **c** – $1250\text{--}50\text{ cm}^{-1}$ region collected in the $E \parallel c$ polarization geometry with an inset with $E \perp c$. The experimental spectrum is shown by dots. The curve matching the dots is a result of a spectral fit as a sum of individual Voigt peaks shown below the curve.

3.3. Vibrations of UO_2^{2+}

The intense infrared band at 925 cm^{-1} and the shoulder at 905 cm^{-1} are connected with the ν_3 antisymmetric stretching mode of $(UO_2)^{2+}$. The presence of a very weak band at 951 cm^{-1} in the Raman spectrum can also be attributed to the same vibrational mode, indicating a slight asym-

metry of the O–U–O unit. Similarly, a low-intense band was also observed in zincorietveldite (Kampf et al. 2023).

The ν_1 symmetric stretching vibration of $(UO_2)^{2+}$ can be attributed to a weak infrared band at 858 cm^{-1} , whereas in the Raman spectra, this vibrational mode is represented by a prominent band at 861 cm^{-1} . The presence of shoulders at 853 and 842 cm^{-1} reflects a slight

ν_1 mode splitting. The U–O bond length obtained from the ν_1 (UO_2)²⁺ stretching energy is, using the relation of Bartlett and Cooney (1989), 1.76 Å for 853 cm⁻¹. For the band at 842 cm⁻¹, the value is 1.77 Å, which is slightly more than that obtained from the refined structure. It is then possible that this band adheres to a different mode (e.g., associated with vibrations of molecular water).

Very weak bands at 317 and 330 cm⁻¹, observed only in the E ⊥ c polarization geometry, can be attributed to the U–O_{eq} stretching modes.

Bands at 273 and 219 cm⁻¹ are assigned to the doubly degenerate ν_2 bending vibration of the (UO_2)²⁺ cation.

3.4. Combination modes, overtones and lattice vibrations

The low-intensity infrared bands at 1792, 1461, and 1430 cm⁻¹ are attributed to overtones and combination modes, respectively.

Raman bands at 193, 173, 154, 123, 95, 84 cm⁻¹ are attributed to the lattice vibrations.

4. Chemical composition

Chemical composition was analyzed from a carbon-coated, polished section using a Cameca SX100 electron microprobe operating in wavelength-dispersive spectroscopy mode at an accelerating voltage of 15 kV, beam current of 4 nA, and a beam diameter of 8 μm. Standards used for calibration include: synthetic UO_2 (U), SrSO_4 (S), gahnite (Zn), forsterite (Mg), wollastonite (Ca), hematite (Fe), lammerite (Cu), and metallic Ni (Ni). Raw X-ray intensities were corrected for matrix effects with a $\phi(\rho z)$ algorithm of *X-PHI* routine (Merlet 1994) involving a theoretical amount of water for calculations.

The analyzed crystal shows slightly variable chemical composition, particularly in Mg for Zn substitution, and can be characterized by the following empirical formula ($n = 8$): $(\text{Mg}_{0.63}\text{Zn}_{0.22}\text{Cu}_{0.09}\text{Fe}_{0.05})_{\Sigma 0.99}(\text{UO}_2)(\text{SO}_4)_2 \cdot 5\text{H}_2\text{O}$.

5. X-ray crystallography, structure refinement, and structure description

An 80 × 40 × 15 μm crystal fragment of synthetic “magnesiorietveldite” was selected under an optical microscope and mounted on a glass fiber for X-ray study using a Rigaku SuperNova diffractometer. For the diffraction experiment, we utilized the $\text{MoK}\alpha$ radiation ($\lambda = 0.71073$ Å) from a micro-focus X-ray tube collimated and monochromatized by mirror optics and detected by an Atlas S2 CCD detector. Synthetic “magnesiorietveldite”, similar to the homeotypic compounds, is orthorhombic, space group $Pmn2_1$, with $a = 12.7950(9)$, $b = 8.3288(4)$, $c = 11.2962(4)$ Å, $V = 1203.80(11)$ Å³, and $Z = 2$. Integration of the diffraction data, including corrections for background, polarization and Lorentz effects, and absorption correction (multi-scan + sphere), was carried out with the CrysAlis RED program (Rigaku, 2025) and Jana2020 (Petříček et al. 2023), respectively. Crystallographic data, experimental and refinement details are given in Tab. 1. The crystal structure was refined from starting coordinates reported for zincorietveldite by Kampf et al. (2023), employing the software Jana2020, running the full-matrix least-squares refinement based on F^2 . Due to

Table 1. Data collection and structure refinement details for synthetic “magnesiorietveldite”.

Structural formula	$(\text{Mg}_{0.716}\text{Zn}_{0.284})(\text{UO}_2)(\text{SO}_4)_2(\text{H}_2\text{O})_5$
Unit-cell parameters	
a, b, c [Å]	12.7950(9), 8.3288(4), 11.2962(4)
V [Å ³]	1203.80(11)
Z	2
Space group	$Pmn2_1$ (#31)
D_{calc} (g cm ⁻³)	3.190 (without H atoms)
Temperature	297 K
Wavelength	$\text{MoK}\alpha$, 0.71073 Å
Crystal dimensions	0.08 × 0.04 × 0.02 mm
Collection mode	ω scans to fill an Ewald sphere
Frame width, counting time	0.75, 72 s
Limiting θ angles	2.41–29.74°
Limiting diffraction indices	$-17 < h < 17, -11 < k < 11, -15 < l < 15$
No. of reflections	51,058
No. of unique reflections	3399
No. of observed reflections (criterion)	3113 [$I > 3\sigma(I)$]
Absorption correction (mm ⁻¹), method	14.50, sphere
$T_{\text{min}}/T_{\text{max}}$	0.298/0.316
R_{int} , Completeness to θ_{max}	0.0311, 97%
F_{000}	1043
Parameters, constraints, restraints	186, 13, 0
R_1, wR_2 (obs)	0.0168, 0.0420
R_1, wR_2 (all)	0.0195, 0.0433
GOF (obs, all)	1.32, 1.34
Weighting scheme, weights	$\sigma, 1/(\sigma^2(F_o^2) + 0.02P^2); P = (F_o^2 + 2F_c^2)/3$
$\Delta\rho_{\text{min}}, \Delta\rho_{\text{max}}$ (e.Å ⁻³)	-0.58, 0.55
Flack parameter; No. of Friedel pairs	0.019(5), 1581

Table 2. Selected bond distances (Å) and polyhedral measures for synthetic “magnesianrietveldite”.

U1–O10	1.757(3)	S1–O2	1.442(3)	S2–O6	1.433(3)
U1–O11	1.760(3)	S1–O3	1.465(3)	S2–O7	1.451(5)
U1–O7	2.327(5)	S1–O4	1.486(3)	S2–O8	1.461(4)
U1–O4	2.348(3)	S1–O5	1.489(3)	S2–O9	1.465(4)
U1–O9	2.356(4)	<S1–O>	1.471	<S2–O>	1.453
U1–O5	2.391(3)	ECoN	3.976	ECoN	3.990
U1–O12	2.486(3)	Δ	0.0115	Δ	0.00721
<U1–O _{Ur} >	1.759	Bond-angle variance	7.0439 deg. ^{^2}	Bond-angle variance	1.4956 deg. ^{^2}
<U1–O _{eq} >	2.382				
Mg1/Zn1–O1	2.044(4)	Mg2/Zn2–O14	2.040(6)	Mg1/Zn1 occ.	0.572/0.428
Mg1/Zn1–O8	2.049(3)	Mg2/Zn2–O13	2.054(6)	Mg2/Zn2 occ.	0.860/0.140
Mg1/Zn1–O8	2.049(3)	Mg2/Zn2–O6	2.070(3)		
Mg1/Zn1–OW1	2.072(6)	Mg2/Zn2–O6	2.070(3)		
Mg1/Zn1–O17	2.109(6)	Mg2/Zn2–O16	2.084(6)		
Mg1/Zn1–Ow2	2.210(6)	Mg2/Zn2–O15	2.099(5)		
<Mg1/Zn1–O>	2.089	<Mg2/Zn2–O>	2.070		
<i>V</i> _{Mg1/Zn1}	11.99 Å ³	<i>V</i> _{Mg2/Zn2}	11.77 Å ³		
ECoN	5.839	ECoN	5.981		
Δ	0.02262	Δ	0.00729		
O12–O13	3.069(2)	O15–O17	2.793(2)	O18–O8	2.8498(17)
O12–O18	2.9804(19)	O15–O2	2.767(2)	O19–O20	2.8338(19)
O12–O22	2.730(3)	O16–O17	2.9554(18)	O19–O21	2.840(2)
O13–O8	2.7995(17)	O16–O17	3.1543(18)	O19–O5	2.8193(18)
O13–O15	3.004(2)	O16–O18	2.8613(17)	O19–O6	3.1190(17)
O14–O15	2.883(2)	O17–O21	2.693(2)	O21–O22	3.013(3)
O14–O20	2.8878(19)	O18–O6	3.0667(16)		
O14–O22	2.894(2)	O18–O6	2.8450(16)		

Table 3. Bond-valence analysis for synthetic “magnesianrietveldite” (values are given in valence units, *vu*).*

	U1	M1	M2	S1	S2	sum ^H	assign.	sum ^H	theor ^[H]	<i>n</i> H ₂ O
O1		0.38				0.38	H ₂ O	1.98	2 ^s	1
O2				1.62		1.62	O			
O3				1.53		1.53	O	1.93	2 ^w	
O4	0.53			1.45		1.98	O			
O5	0.48			1.44		1.92	O			
O6			0.35 ^{*21}		1.65	2.01	O			
O7	0.55				1.58	2.13	O			
O8		0.38 ^{*21}			1.54	1.92	O			
O9	0.52				1.53	2.05	O			
O10	1.84					1.84	O			
O11	1.83					1.83	O			
O12	0.39					0.39	H ₂ O	1.99	2 ^s	2
O13			0.37			0.37	H ₂ O	1.97	2 ^s	1
O14			0.38			0.38	H ₂ O	1.98	2 ^s	1
O15			0.33			0.33	H ₂ O	1.93	2 ^s	1
O16			0.34			0.34	H ₂ O	1.94	2 ^s	1
O17		0.33				0.33	H ₂ O	1.93	2 ^s	1
Ow1		0.36				0.36	H ₂ O	1.96	2 ^s	1
Ow2		0.26				0.26	H ₂ O	1.86+0.2 [#]	1 ^w	1
sum	6.15	2.08	2.13	6.03	6.30					10

* Bond-valence parameters are from Gagné and Hawthorne (2015). sum^H – the sum of the BV without the contribution of the H bonds; sum^H – the sum of the BV including assumed H bonds (considering the theoretical H-bond strength of 0.8*vu* for the *D*–H bond and 0.2 *vu* for the H–*A* bond, after Brown 2002); *n*H₂O – number of H₂O molecules/cell, considering site-multiplicities and *Z* = 4; # – indicates that it can go about a *non-transformer* with ^[4]O atom.

the non-centrosymmetric space group, the crystal was modeled as an inversion twin, giving a low fraction of the second-twin domain, thus representing the correct enantiomorph (Tab. 1). The Mg1 and Mg2 sites were refined with joint occupancies by Mg and Zn, yielding Mg1_{0.572(5)}Zn1_{0.428(5)} and Mg2_{0.860(5)}Zn2_{0.140(5)}, respectively. These correspond to site scattering values of 39.53 and 29.04, respectively, for a total site scattering of 68.57. For comparison, the total site-scattering value corresponding to full site occupancies with the cation ratios indicated by the electron probe microanalyses is 73.68. The final refinement cycles, including refinement of anisotropic displacement parameters for nearly all atoms (except one O of the H₂O group; some of the H atoms – corresponding maxima – were visible from the

difference-Fourier maps but unlocalized), converged to $R=0.0168$ for 3113 unique reflections with $I>3\sigma(I)$ and $wR_2=0.0433$ for all 3399 reflections (Tab. 1). Selected bond distances and geometrical measures are given in Tab. 2, and bond-valence analysis is in Tab. 3. The bond-valence analysis was done following Brown's standard procedure (2002), using the bond-valence parameters taken from Gagné and Hawthorne (2015) and Brown (2002).

"Magnesorietveldite" is isostructural with rietveldite and zincorietveldite. The degree of structural similarity between the structures was checked using the COMPSTRU (de la Flor et al. 2016) utility within the Bilbao Crystallographic Server. The results are given in Tab. 4, which documents the isostructurality of those minerals.

The U site in the structures (Fig. 7a) of the rietveldite subgroup of minerals is coordinated by seven O atoms forming a UO_7 pentagonal bipyramid, the most typical coordination for U^{6+} in solids, particularly in uranyl sulfates. The U^{6+} and two O^{2-} with short apical bonds constitute the uranyl group, UO_2^{2+} . Four of the five equatorial O atoms of the UO_7 bipyramid are linked to SO_4 tetrahedra; the other is an H_2O group (see BV table). The linkages of pentagonal bipyramids and tetrahedra form an infinite $[(UO_2)(SO_4)_2(H_2O)]^{2-}$

chain along [001] (Fig. 5b). The chains are linked in the [100] direction by $M1O_2(H_2O)_4$ and $M2O_2(H_2O)_4$

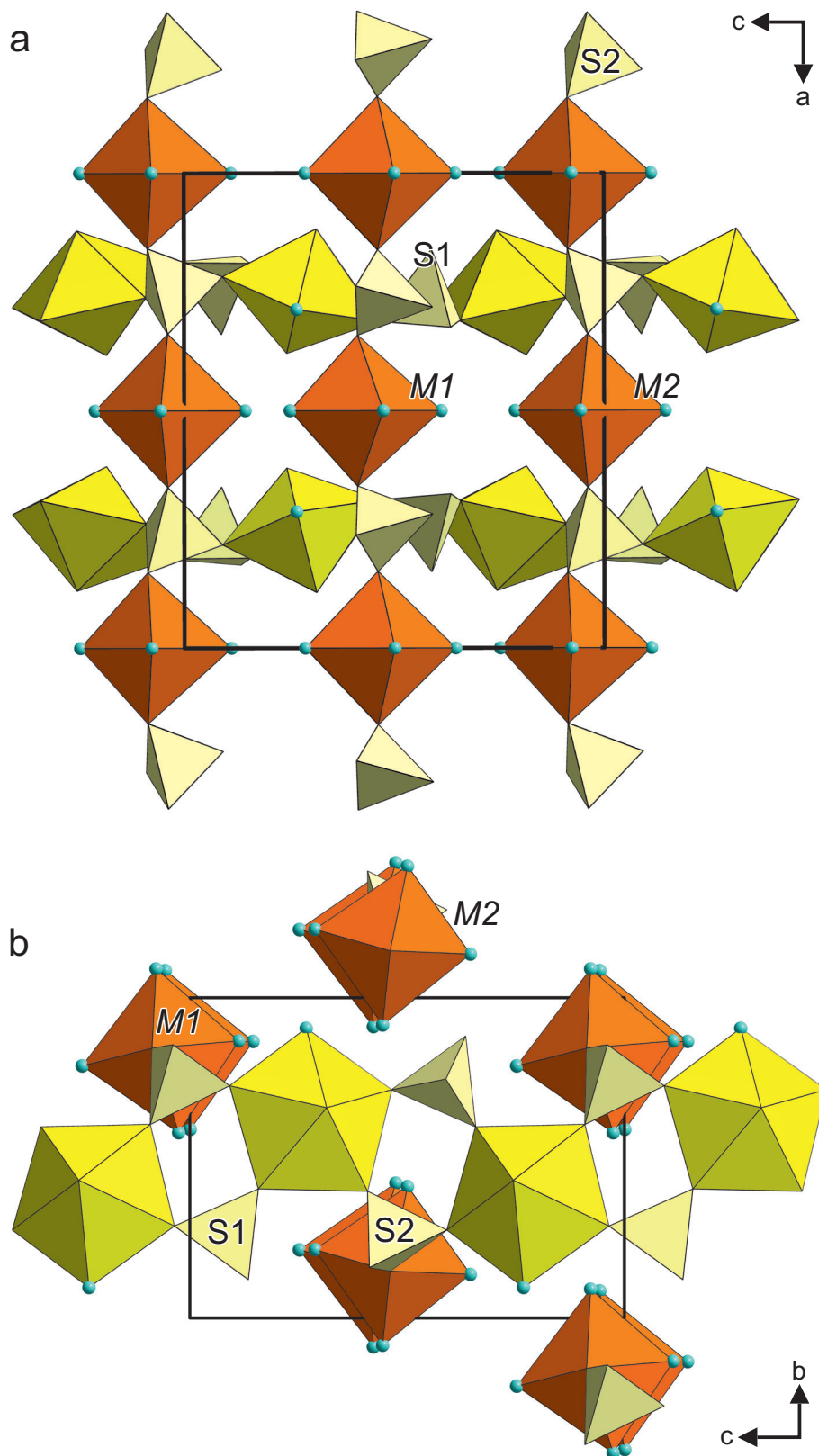


Fig. 7 Crystal structure of synthetic "magnesorietveldite". **a** – Structure viewed down [010]. UO_7 – yellow, SO_4 – pale yellow, $M1/M2$ octahedra – orange, H_2O molecules represented by blue circles. **b** – Infinite chain of the composition $[(UO_2)(SO_4)_2(H_2O)]^{2-}$, which is a common feature for all svornostite-group minerals as well as for other uranyl sulfate minerals (its geometrical isomer, respectively). Color scheme is the same for both figures.

Table 4. Results of the COMPSTRU procedure for the structure comparison of rietveldite, zincorietveldite and synthetic “magnesorietveldite”.

	Rietveldite/synth. “magnesorietveldite”	Rietveldite/Zincorietveldite
S	0.0043	0.0023
d_{\max} (Å)	0.0888	0.0903
d_{av} (Å)	0.0393	0.0244
δ	0.032	0.016

S – the degree of lattice distortion is related to the spontaneous strain (the square root of the sum of the squared eigenvalues of the strain tensor divided by 3).

d_{\max} – corresponds to the maximum difference between the atomic positions of the matching atoms.

d_{av} – of the differences between the atomic positions of the matching atoms.

δ – a function of the differences in atomic positions (weighted by the multiplicities of the sites) and the ratios of the corresponding lattice parameters of the structures. The program does NOT standardize the structure descriptions to calculate δ , and may therefore differ in some cases from the Δ calculated following the procedure of Bergerhoff et al. (1999).

octahedra ($M1 = \text{Mg}1_{0.572(5)}\text{Zn}1_{0.428(5)}$; $M2 = \text{Mg}2_{0.860(5)}\text{Zn}2_{0.140(5)}$), which share O vertices with SO_4 tetrahedra in the chains (Figs 7a, b), resulting in a heteropolyhedral sheet parallel to $\{010\}$. The structural formula obtained from the refinement and bond-valence considerations is $(\text{Mg}_{0.716}\text{Zn}_{0.284})(\text{UO}_2)(\text{SO}_4)_2(\text{H}_2\text{O})_5$, $Z = 2$. The presence of slightly larger $^{[6]}\text{Zn}^{2+}$ (0.744 Å with an average Zn–O bond-length of 2.110 Å), compared to $^{[6]}\text{Mg}^{2+}$ (0.723 Å with an average Mg–O bond-length of 2.089 Å) (Hawthorne and Gagné 2024), is reflected by somewhat larger Mg2/Zn2 (designated $M2$) polyhedral volume and slightly larger irregularity (see the distortion index on bond lengths and ECoN; Tab. 2). Interestingly, in reference to polyhedral measures, the S2 tetrahedron is more regular than the S1 tetrahedron; the S2 tetrahedron is linked to two metal-sites in the interlayer, while the S1 has a *free-vertex*, the O3 atom, which is not linked to the metal site and receives two weak H bonds instead.

The infinite $[(\text{UO}_2)(\text{SO}_4)_2(\text{H}_2\text{O})]^{2-}$ chain in the structures of synthetic “magnesorietveldite”, rietveldite, and zincorietveldite has also been found in the structures of bobcookite, $\text{Na}(\text{H}_2\text{O})_2\text{Al}(\text{H}_2\text{O})_6[(\text{UO}_2)_2(\text{SO}_4)_4(\text{H}_2\text{O})_2] \cdot 8\text{H}_2\text{O}$ (Kampf et al. 2015a), oldsite, $\text{K}_2\text{Fe}[(\text{UO}_2)(\text{SO}_4)_2]_2 \cdot 8\text{H}_2\text{O}$ (Plášil et al. 2023), oppenheimerite, $\text{Na}_2(\text{H}_2\text{O})_2[(\text{UO}_2)(\text{SO}_4)_2(\text{H}_2\text{O})]$ (Kampf et al. 2015b), svornostite, $\text{K}_2\text{Mg}[(\text{UO}_2)(\text{SO}_4)_2]_2 \cdot 8\text{H}_2\text{O}$ (Plášil et al. 2015), synthetic $\text{K}_2[(\text{UO}_2)(\text{SO}_4)_2(\text{H}_2\text{O})](\text{H}_2\text{O})$ (Ling et al. 2010) and synthetic $\text{Mn}(\text{UO}_2)(\text{SO}_4)_2(\text{H}_2\text{O})_5$ (Tabachenko et al. 1979). The chains in bobcookite and oppenheimerite are geometrical isomers of the chain in oldsite, rietveldite, and zincorietveldite structures.

6. Discussion and concluding remarks

6.1. Structural relationships

The structures of $M^{2+}[(\text{UO}_2)(T^{6+}\text{O}_4)_2(\text{H}_2\text{O})](\text{H}_2\text{O})_4$ family of synthetic compounds have been studied in detail by Gurzhiy et al. (2019) and Korniyakov et al. (2021).

Based on a series of synthetic experiments, providing a suite of either pure compounds (reflecting M -sites and/or T -sites within the structure) with different M -cations (Mg, Mn, Fe, Co, Ni, and Zn) and/or T -sites cations (S or Se), they provided several general conclusions. There are three known structural types with topologically identical U-containing infinite chains that can be described as polytypes. The Mg^{2+} bearing compounds, with the increase of Se-content in the structure, crystallize in all three types starting from the $1M$ polytype (pure uranyl sulfate), through $2O$ (uranyl mixed sulfate–selenate) to the $2M$ polytype (pure uranyl selenate). Gurzhiy et al. (2019) suggested that the changes in the tetrahedral volume lead to the transition of both end-member phases to a more stable orthorhombic modification. At the same time, pure Ni-bearing uranyl sulfate crystallizes as a $2O$ polytype, and the Ni-bearing pure uranyl selenate (Gurzhiy et al. 2017) as a $2M$ polytype. Moreover, Zn-bearing pure uranyl sulfate (Gurzhiy et al. 2019) crystallizes as a $2O$ polytype as well. The difference between the $1M$ and $2O$ polytypes lies in the rotation of the $(\text{T}1\text{O}_4)$ tetrahedra in the adjacent pseudo-layers. They described it as a “*head-to-tail*” or “*head-to-head*” geometry for the $1M$ and $2O$ polytypes, respectively. As an obvious explanation for such a transition between the two polytypes in the Mg-bearing system, they ascribed it to the Se-for-S substitution at the $T1$ site (since the $T2$ site is less responsive to compositional variations; see description of the structure). However, this assumption has been challenged during the comparison of the Se distribution at the $T1$ site within the Mg- and Ni-bearing phases: the dynamics of the Se distribution are the same in both series of compounds (!). Therefore, the conclusion of Korniyakov et al. (2021) is that not only the size of tetrahedral oxyanions, but the radii of divalent metal cations (= Ni, Mg, Zn, Co, Fe, and Mn) are responsible for the crystallization of a particular polytype.

We have undertaken the refinement in this space group ($P2_1$), which is a subgroup of $Pmn2_1$, and the refinement includes merohedral twinning due to the group $>$ subgroup relationship (mirror in $[001]$). The refinement did

not yield a reliable result, yielding R -factors similar to those from the orthorhombic space-group refinement, and some of the anisotropic atomic displacement parameters of the oxygen atoms were incorrectly described. Therefore, we are convinced that the phase studied by us is orthorhombic, space group $Pmn2_1$ (2O polytype). As our compound is purely sulfate and no significant substitution was observed at the T -site, we should consider the main effect on symmetry to be due to divalent cations. The Mg1 (0.5, y , z) site contains nearly 50 : 50 Mg : Zn, while Mg2 (0, y , z) contains nearly 90 : 10 Mg : Zn. The Mg2–O bond lengths (Tab. 2) are consistent with the presence of a slightly smaller cation than at the Mg1 site.

6.2. Weakly bonded constituents in the structures of the svornostite group of minerals: A bond-valence approach

In order to evaluate the crystal structures of oxysalt minerals, with respect to weakly-bonded constituents (such as molecular water) in particular, a so-called *bond-valence approach* has been developed by Frank Hawthorne and his co-workers (see e.g., Hawthorne 1992, 2012, 2015; Hawthorne and Schindler 2009; Schindler and Hawthorne 2008). This theory stems from the rigorous base of the bond-valence theory, one of the theories of chemical bonding (Brown 2023). Using the bond-valence approach, we can inspect, evaluate, and predict how and why the particular structural units and interlayer/interstitial complexes are organized and interacting (in terms of bonding). One of the fundamental principles of bond-valence theory states that stable crystal structures form when the Lewis basicity (LB) of the structural unit (SU) matches the Lewis acidity (LA) of the interstitial complex (IN). Both values are affected by several facts; nevertheless, we must emphasize the specific roles of hydrous species (H_2O and OH^-) present within the SU . The presence of H_2O (and, namely, that of so-called *transformer* H_2O , with ^{13}O) affects both the dimensionality of the oxysalt structures and effectively reduces the LA of the cation to which it is bonded. The theory enables the prediction of the total number of H_2O molecules in the structure based on bond-valence requirements and typological distinctions. In the following paragraphs, we use the specific terminology of the bond-valence approach. For those unfamiliar with it and the calculations, refer to the original papers by Frank Hawthorne and co-workers.

The svornostite group of minerals, as established by Kampf et al. (2025), comprises two subgroups: rietveldite (with rietveldite and zincorietveldite; and here also “magnesorietveldite”) and svornostite (with svornostite-(K), svornostite-(NH_4), and oldsite-(K) as members). All of the above-mentioned members are based on the same fundamental building units/structural units; nevertheless,

they differ in the metal cation content in the interlayer and in the total number of H_2O molecules hosted in the structure. Interestingly, rietveldites have four water molecules (per 1 U) in the interlayer complex, and svornostites have only three. We would also like to examine the types and the role of the H_2O in their crystal structures.

The crystal structures of svornostite-group minerals all possess $[(UO_2)(SO_4)_2(H_2O)]^{2-}$ structural units and an interlayer complex that can be simplified as $Me_2^+Me^{2+}(H_2O)_3$ (svornostites) and $Me^{2+}(H_2O)_4$ (rietveldites). The *charge deficiency per anion* (CDA) of the structural unit is 0.22 vu . The CDA is an important measure expressing the average *bond-valence* per O atom contributed by the interstitial species and adjacent structural units. It correlates strongly with the average O-coordination number of the structural unit. We can compare the value of the CDA of svornostite-group minerals with the range of CDA of structural units for uranyl sulfates listed by Plášil et al. (2023): 0.15–0.25 vu . Now, following the approach of Schindler and Hawthorne (2008), we can calculate the Lewis basicity (LB) of the structural unit of the svornostite-group minerals, which falls within the range 0.14–0.23 vu . From the valence-matching principle of the bond-valence theory, we know that from the possible interstitial complexes, only those will form the stable structures when matching the same range; the Lewis acidity (LA) of interstitial complexes should lie in the range of 0.14–0.23 vu .

In general, the formula of the interstitial complex can be written as (Schindler and Hawthorne 2008): $^{[m]}M^+_a$ $^{[n]}M^{2+}_b$ $^{[l]}M^{3+}_c$ $(H_2O)_d$ $(H_2O)_e$ $(H_2O)_f$ $^{[q]}(OH)_g$ $(H_2O)_r$ $^{(a+2b+3c-l)+}$, where M is any type of interstitial cation, d , e , and f denote the numbers of *transformer*, *non-transformer* and *inverse transformer* (H_2O) groups, and r denotes the number of interstitial (H_2O) groups not bonded to interstitial cations. The Lewis acidity of the interstitial complex is defined as *its effective charge divided by the number of bonds from the interstitial complex to the structural unit* (Schindler and Hawthorne 2008). The effective charge of the interstitial complex can be derived from the formula given above: it is the formal charge, $a+2b+3c-g$, as modified by the H bonds emanating from the structural unit, $h \times s$, where h is the strength of a hydrogen bond (~ 0.2 vu). To determine s , the number of H bonds emanating from the structural unit, we need to know the structural unit to be considered. The number of bonds from the interstitial complex to the structural unit may be counted from the above formula as the number of bonds emanating from the cations, $m \times a + n \times b + l \times c$, plus the number of bonds resulting from the transformer action of H_2O , d , minus the number of bonds accepted by (OH) groups in the interstitial complex, $g \times [q-1]$, plus the number of H bonds emanating from the structural unit, s .

Let us now analyze the interstitial complexes in the svornostite group of minerals, using rietveldite (Kampf et al. 2017) as an example. In sum, the interstitial complex in rietveldite is $\{^{[6]}\text{Fe}^{2+}(\text{H}_2\text{O})_4\}^{2+}$, where (H_2O) should all be of the transformer type, and there are two H bonds emanating from the structural unit (1 H_2O with SU), then the LA of the interstitial complex in rietveldite should equal to: $2+2 \times 0.2$ (effective charge) = 2.4+. The number of bonds from the interstitial complex to the structural unit is 6 (from Fe) + 4 [from transformer (H_2O) groups] + 2 (H bonds to the interstitial complex due to 1 H_2O within SU) = 14. Thus, the Lewis acidity of the rietveldite interstitial complex is $2.4/12 = 0.20 \text{ vu}$. Similarly, we can calculate the LA value for zincrietveldite and synthetic “magnesianrietveldite”, which are of the same magnitude. We can compare this number with the LB obtained above, and we see that the two overlap and are near the lower end of the range; nevertheless, they still obey the valence-matching principle.

A more interesting situation occurs in the svornostite subgroup of the svornostite group. In addition to the divalent cation, we have monovalent potassium or the NH_4^+ group here – cations that act as weak Lewis acids. This should also be reflected in the type of (H_2O) present in the interstitial complexes of the svornostite subgroup. Let us now analyze the interstitial complex in svornostite $\text{K}_2\text{Mg}[(\text{UO}_2)_2(\text{SO}_4)_4(\text{H}_2\text{O})_2](\text{H}_2\text{O})_6$ (Plášil et al. 2015). The interstitial complex in svornostite comprises $\{^{[9]}\text{K}^+ [^{11}]\text{K}^+ [^{6}]\text{Mg}^{2+} (\text{H}_2^{[3]}\text{O})_2(\text{H}_2\text{O})_4\}^{4+}$, where two of the (H_2O) groups, bonded to Fe, are of the transformer type, and four H bonds are emanating from the structural unit (2 H_2O within SU). However, a closer inspection of the bond-valence analysis results reported in the original

paper drives us to the conclusion that both O11 and O14 (H_2O) are inverse-transformer (H_2O) groups with [5]-coordinated O atoms. For instance, O11: with two bonds, it is bonded to K1 and K2, two strong H bonds (as H_2O), and it should accept one weak H bond ($\sim 0.2 \text{ vu}$) in addition, to satisfy its bond-valence requirements ($S_{\text{K1}} + S_{\text{K2}} + 2 \times H_{\text{strong}} = 0.08 + 0.13 + 1.6 = 1.81 \text{ vu}$; leaving a bond-strength of 0.19 vu free for accepting a weak H bond). The effective charge is 4.8+. The number of bonds from the interstitial complex to the structural unit is 20 (from K) + 6 (from Mg) + 2 [from transformer (H_2O) groups] + 4 (H-bonds to the interstitial complex) – 2 (action of inverse-transformer H_2O) = 30. Thus, the Lewis acidity of the svornostite interstitial complex is $4.8/32 = 0.16 \text{ vu}$. We can compare this number with the LB obtained above; they overlap and fall within the range, yet still obey the valence-matching principle.

The interstitial complex in svornostite- (NH_4) (Kampf et al. 2025) can be written as $\{^{[11]}\text{N}1\text{H}_4^+ [^{9}]\text{N}2\text{H}_4^+ [^{6}]\text{Mg}^{2+} (\text{H}_2^{[3]}\text{O})_2(\text{H}_2\text{O})_4\}^{4+}$, where two of the (H_2O) groups, bonded to Mg (based on the BV analysis given in the original paper), are of the transformer type and they will affect the number of bonds from the interstitial complex to adjacent structural unit; plus there are four H bonds are emanating from the structural unit (2 H_2O within SU). The LA of the interstitial complex in svornostite- (NH_4) should equal: $4+4 \times 0.2$ (effective charge) = 4.8+. The number of bonds from the interstitial complex to the structural unit is 20 (from N) + 6 (from Mg) + 2 [from transformer (H_2O) groups] + 4 (H bonds to the interstitial complex) – 4 (effect of the inverse-transformer (H_2O) groups) = 32. The NH_4^+ behaves like a weak Lewis acid, similar to K^+ or Cs^+ ($LA_{\text{NH}_4^+} = 0.11 \text{ vu}$). Thus, it does not

link to any transformer (H_2O) group (see Tab. 6 in Kampf et al. 2025), but instead the (H_2O) groups bonded to N sites in svornostite- (NH_4) act as inverse-transformer groups, with each of them, two bonds to two N sites + two strong H bonds (donated) + one weak H bond ($\sim 0.2 \text{ vu}$) accepted. Hence, the

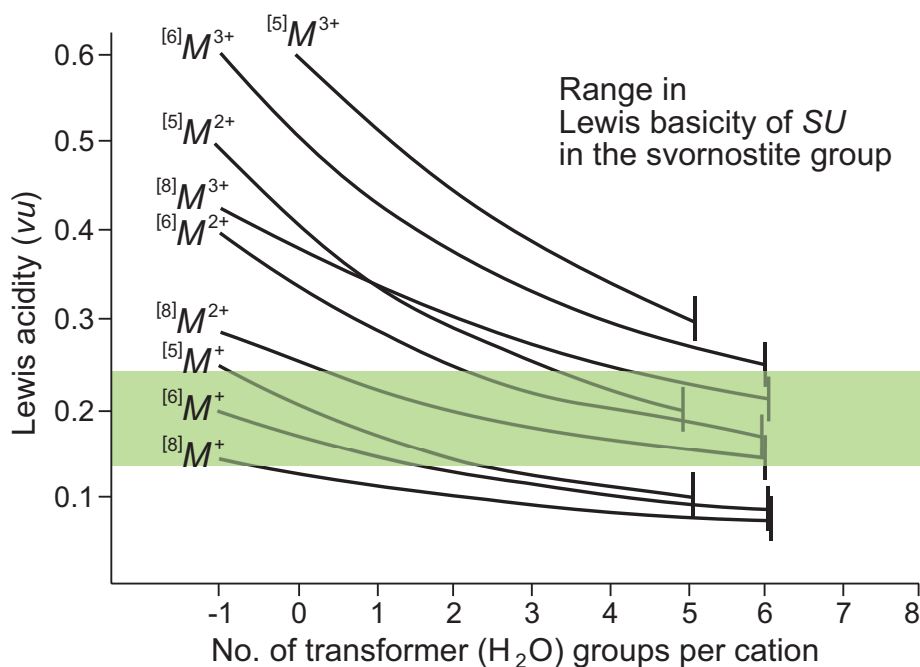


Fig. 8 The variation in Lewis acidity with the number of transformer (H_2O) groups for different interstitial-cation charges and coordination numbers for a general interstitial complex; the range in Lewis basicity of the structural unit of the svornostite group of minerals, $[(\text{UO}_2)(\text{H}_2\text{O})(\text{SO}_4)_2]^{2-}$, is marked in light green; where the lines of variable Lewis acidity overlap the range of Lewis basicity of the structural unit, the valence-matching principle is obeyed.

Lewis acidity of the svornostite interstitial complex is $4.8/28 = 0.17$ *vu*, which matches.

We can compare our considerations against the plot shown in Fig. 8. The valence-matching principle, demonstrated by the overlap of the *LB* and *LA* of the structural unit and the interstitial complex, holds for the four transformer H₂O groups observed in the structure. Moreover, we can see that such a weak Lewis acid as NH₄⁺ should not be bonded to any of the transformer (H₂O) groups.

Schindler and Hawthorne (2008) introduced an interesting measure: the ratio of the number of anions in the structural unit to the number of bonds emanating from interstitial cations and (OH) groups within the structural unit, which dictates the number and types of (H₂O) groups in the interstitial complex. This ratio is called a *bond-valence distribution factor (D)*. It is defined as follows: $D = (N^{A:SU}) / [(N^{B:IC}) + (N^{(OH):SU})]$, where $N^{A:SU}$ is the number of anions (A) in the structural unit (SU), $N^{B:IC}$ is the number of bonds (B) emanating from the interstitial complex (IC), and $N^{(OH):SU}$ is the number of (OH) groups in the structural unit. Following the paper (Schindler and Hawthorne 2008), the critical factors controlling the number of bonds emanating from an interstitial complex are **(1)** the number of (OH)⁻ groups bonded to interstitial cations, and **(2)** the number of inverse-transformer (H₂O) groups. Both groups reduce the number of bonds emanating from the interstitial cations and, therefore, both groups affect the number of interstitial (H₂O) groups. For each bond removed by the action of an (OH) group or inverse bond-valence transformer (H₂O) group, an additional (H₂O) group (transformer or nontransformer) may be required to distribute the bond valence to the anions of the structural unit. For rietveldites, the bond-valence distribution factor is 1.83 ($D = 11/6$). The total number of predicted H₂O groups is 6, and 4 transformer groups per cation (following equations (4) and (7); check also figures 8a, c *in* Schindler and Hawthorne 2008). This aligns with our experimental structure data. The situation for the svornostite-subgroup members is more complicated; the bond-valence distribution factor is 0.85 ($D = 22/26$). The total number of H₂O groups predicted is 1, which is somewhat outlying, but the predicted number of transformer H₂O groups is 0. This is in line with Fig. 7, which shows that the cation with coordination number higher than [8] must be bonded to one or more inverse-transformer groups. This is consistent with the bond-valence analysis of the svornostite-(K) and svornostite-(NH₄) structures (see, e.g., Tab. 6 *in* Kampf et al. 2025). To sum up, the structures discussed here have the same overall molecular (H₂O) content, but the role and type of (H₂O) groups in rietveldite- and svornostite-type structures are distinct.

Acknowledgments: We thank Stefan Ansermet for the microphotography of the studied specimen, which is very difficult to photograph. The helpful comments of Vlad Gurzhiy and Sergey Krivovichev are highly acknowledged, as well as those by the handling editor and Editor-in-Chief. This study was supported by the CzechNanoLab Research Infrastructure, supported by MEYS CR (LM2023051) (JP) and by the support of the OP VVV project (Geobarr CZ.02.1.01/0.0/0.0/16_026/008459 for RS).

References

- BARTLETT JR, COONEY RP (1989) On the determination of uranium-oxygen bond lengths in dioxouranium(VI) compounds by Raman spectroscopy. *J Mol Struct* 193: 295–300
- BERGERHOFF G, BERNDT M, BRANDENBURG K, DEGEN T (1999) Concerning inorganic structure types. *Acta Crystallogr B* 55: 147–156
- BROWN ID (2002) The chemical bond in inorganic chemistry: the bond valence model. Oxford University Press, UK, pp 1–278
- BROWN ID (2023) A rigorous theory of valence. *Struct Chem* 34: 361–389
- BRUGGER J, MEISSER N, BURNS PC (2003) Contribution to the mineralogy of acid drainage of uranium minerals: maretite and the zippeite-group. *Am Mineral* 88: 676–685
- ČEJKA J (1999) Infrared spectroscopy and thermal analysis of the uranyl minerals. *IN: BURNS PC, EWING RC (eds) Uranium: Mineralogy, geochemistry and the environment. Rev Min Geochem* 38, Mineralogical Society of America, pp 521–622
- ČEJKA J, FROST R, SEJKORA J, KEEFFE E (2009) Raman spectroscopy study of the uranyl sulphate mineral jáchymovite (UO₂)₈(SO₄)(OH)₁₄·13 H₂O. *J Raman Spectrosc* 40: 1464–1468
- DE LA FLOR G, OROBENGOA D, TASCI E, PEREZ-MATO J M, AROYO MI (2016) Comparison of structures applying the tools available at the Bilbao Crystallographic Server. *J Appl Crystallogr* 49: 653–664
- GAGNÉ OC, HAWTHORNE FC (2015) Comprehensive derivation of bond-valence parameters for ion pairs involving oxygen. *Acta Crystallogr B* 71: 562–578
- GURZHIY VV, PLÁŠIL J (2019) Structural complexity of natural uranyl sulfates. *Acta Crystallogr B* 75: 39–48
- GURZHIY VV, TYUMENTSEVA OS, KRIVOVICHEV SV, TANANAEV IG (2017) Selective Se-for-S substitution in Cs-bearing uranyl compounds. *J Solid State Chem* 248: 126–133
- GURZHIY VV, TYUMENTSEVA OS, IZATULINA AR, KRIVOVICHEV SV, TANANAEV IG (2019) Chemically Induced Polytropic Phase Transitions in the Mg[(UO₂)(TO₄)₂(H₂O)](H₂O)₄ (T = S, Se) System. *Inorg Chem* 58 (21): 14760–14768

- HAWTHORNE FC (1992) The role of OH and H₂O in oxide and oxysalt minerals. *Z Kristallogr* 201: 183–206
- HAWTHORNE FC (2012) A bond-topological approach to theoretical mineralogy: crystal structure, chemical composition and chemical reactions. *Phys Chem Min* 39(10): 841–874
- HAWTHORNE FC (2015) Toward theoretical mineralogy: A bond-topological approach. *Am Mineral* 100(4): 696–713
- HAWTHORNE FC, GAGNÉ OC (2024) New ion radii for oxides and oxysalts, fluorides, chlorides and nitrides. *Acta Crystallogr B* 80, 326–339
- HAWTHORNE FC, SCHINDLER M (2009) Understanding the weakly bonded constituents in oxysalt minerals. *Z Kristallogr* 223: 41–68
- KAMPF AR, PLÁŠIL J, KASATKIN AV, MARTY J (2015a) Bobcookite, NaAl(UO₂)₂(SO₄)₄·18H₂O, and wetherillite, Na₂Mg(UO₂)₂(SO₄)₄·18H₂O, two new uranyl sulfate minerals from the Blue Lizard mine, San Juan County, Utah, USA. *Mineral Mag* 79: 695–714
- KAMPF AR, PLÁŠIL J, KASATKIN AV, MARTY J, ČEJKA J (2015b) Fermitite, Na₄(UO₂)(SO₄)₃·3H₂O, and oppenheimerite, Na₂(UO₂)(SO₄)₂·3H₂O, two new uranyl sulfate minerals from the Blue Lizard mine, San Juan County, Utah, USA. *Mineral Mag* 79: 1123–1142
- KAMPF AR, SEJKORA J, WITZKE T, PLÁŠIL J, ČEJKA J, NASH BP, MARTY J (2017) Rietveldite, Fe(UO₂)(SO₄)₂(H₂O)₅, a new uranyl sulfate mineral from Giveaway-Simplot mine (Utah, USA), Willi Agatz mine (Saxony, Germany) and Jáchymov (Czech Republic). *J Geosci* 62: 107–120
- KAMPF AR, OLDS TA, PLÁŠIL J, MARTY J (2023) Zincorietveldite, Zn(UO₂)(SO₄)₂(H₂O)₅, the zinc analogue of rietveldite from the Blue Lizard mine, San Juan County, Utah, USA. *Mineral Mag* 87: 528–533
- KAMPF AR, OLDS TA, PLÁŠIL J, MA C, CELESTIAN AJ, MARTY J (2025) Svornostite-(NH₄), (NH₄)₂Mg(UO₂)₂(SO₄)₄(H₂O)₈, a new mineral from the Blue Lizard mine, San Juan County, Utah, USA, and the establishment of the svornostite mineral group. *Mineral Mag* 89(5): 609–617
- KORNYAKOV IV, TYUMENTSEVA OS, KRIVOVICHEV SV, TANANAIEV IG, GURZHIY VV (2021) Crystal chemistry of the M²⁺[(UO₂)(T⁶⁺O₄)₂(H₂O)](H₂O)₄ (M²⁺ = Mg, Mn, Fe, Co, Ni and Zn; T⁶⁺ = S, Se) compounds: the interplay between chemical composition, pH and structural architecture. *Cryst Eng Comm* 23: 1140–1148
- LIBOWITZKY E (1999) Correlation of O-H stretching frequencies and O-H···O hydrogen bond lengths in minerals. *Monatsh Chem* 130: 1047–1059
- LING J, SIGMON GE, WARD M, ROBACK N, BURNS PC (2010) Syntheses, structures, and IR spectroscopic characterization of new uranyl sulfate/selenate 1D-chain, 2D-sheet and 3D framework. *Z Kristallogr* 225: 230–239
- MAJZLAN J, PLÁŠIL J, ŠKODA R, GESCHER J, KÖGLER F, RUSZNYAK A, KÜSEL K, NEU TR, MANGOLD S, ROTHE J (2014) Arsenic-Rich Acid Mine Water with Extreme Arsenic Concentration: Mineralogy, Geochemistry, Microbiology, and Environmental Implications. *Environ Sci Technol* 48 (23): 13685–13693
- MERLET C (1994) An Accurate Computer Correction Program for Quantitative Electron Probe Microanalysis. *Microchim Acta* 114–115: 363–376
- OMNIC 9.2.98; Version 9.2; Thermo Fisher Scientific Inc. 1992–2012
- PETŘÍČEK V, PALATINUS L, PLÁŠIL J, DUŠEK M (2023) Jana2020 – a new version of the crystallographic computing system Jana. *Z Kristallogr* 229: 345–352
- PLÁŠIL J (2014) Oxidation–hydration weathering of uraninite: the current state-of-knowledge. *J Geosci* 59: 99–114
- PLÁŠIL J, SEJKORA J, ŠKODA R, ŠKÁCHA P (2014) The recent weathering of uraninite from the Červená vein, Jáchymov (Czech Republic): a fingerprint of the primary mineralization geochemistry onto the alteration association. *J Geosci* 59: 223–253
- PLÁŠIL J, HLOUŠEK J, KASATKIN AV, NOVÁK M, ČEJKA J, LAPČÁK L (2015) Svornostite, K₂Mg[(UO₂)(SO₄)₂]₂·8H₂O, a new uranyl sulfate mineral from Jáchymov, Czech Republic. *J Geosci* 60: 113–121
- PLÁŠIL J, STECIUK G, MAJZLAN J, ŠKODA R, FILIP J, PETR M, KOLAŘÍK J, KLEMENTOVÁ M, BÄHRE O, KLÖSS G, LAPČÁK L (2022) 3D Electron Diffraction as a Powerful Tool to Study the Earliest Nanocrystalline Weathering Products: A Case Study of Uraninite Weathering. *ACS Earth Space Chem* 6: 1250–1258
- PLÁŠIL J, KAMPF AR, MA C, DESOR J (2023) Oldsite, K₂Fe²⁺[(UO₂)(SO₄)₂]₂(H₂O)₈, a new uranyl sulfate mineral from Utah, USA: its description and implications for the formation and occurrences of uranyl sulfate minerals. *Mineral Mag* 87: 151–159
- RIGAKU (2025) CrysAlis CCD and CrysAlis RED. Rigaku-Oxford Diffraction Ltd, Yarnton, Oxfordshire, UK
- SCHINDLER M, HAWTHORNE FC (2008) The stereochemistry and chemical composition of interstitial complexes in uranyl-oxysalt minerals. *Canad Mineral* 46: 467–501
- SEREZHKIN VN, SEREZHKINA LB (1978) X-ray diffraction study of double uranyl sulphates M(UO₂)(SO₄)·5H₂O. *Russ J Inorg Chem* 23: 414–416
- TABACHENKO VV, SEREZHKIN VI, SEREZHKINA LB, KOVBA LM (1979) Crystal structure of manganese sulfatouranilate MnUO₂(SO₄)₂(H₂O)₅. *Sov J Coord Chem* 5: 1219–1223
- VLČEK V, ČEJKA J, CÍSAŘOVÁ I, GOLIÁŠ V, PLÁŠIL J (2009) Crystal structure of UO₂SO₄·2.5H₂O: Full anisotropic refinement and vibration characteristics. *J Mol Struct* 936: 75–79